Int. J. Solids Structures Vol. 28, No. 6, pp. 691–702, 1991
Printed in Great Britain.

0020–7683/91 $3.00 + .00

BEHAVIOUR OF CYLINDRICAL HIP CONTAINERS

J. BESSON† and M. ABOUAF‡
Ecole Nationale Supérieure des Mines de Paris, Centre des Matériaux P.M. Fourt,
BP 87 Evry Cedex 91003, France

(*Received* 30 *August* 1990; *in revised form* 3 *December* 1990)

Abstract—A simple easy-to-use model for Hot Isostatic Pressing (HIP) with cylindrical containers is proposed. This model provides a simple description of stresses and strains in both the powder and can during the HIP process. The model is also used to prove that the radial shrinkage of the powder is always greater than the axial shrinkage. Results are compared with finite element calculations; the good agreement between the two sets of computations shows that the simplified proposed model realistically describes the HIP process. Finally the model is used to estimate the effects of rheology of the powder and of the can as well as the effects of geometry on the final non-isotropic deformation of the container.

INTRODUCTION

Hot Isostatic Pressing (HIP) is an industrial process which allows the fabrication of high quality metallic and ceramic parts. When the initial powder compact is highly porous, a preform (container) must be used in order to avoid the penetration of the pressurizing gas into the porous channels. Since the applied load (gas pressure) is hydrostatic, the deformation of the porous body is supposed to be isotropic. In practice, the initial and final products differ in scale but also in shape. As shown by Li *et al.* (1987), this can be explained by a non-uniform densification caused by temperature gradients inside the powder due to the low heat conductivity of porous materials. The purpose of this work is to show that inhomogeneous deformation can also be explained by a non-hydrostatic stress state in the powder caused by the stiffness of the container wall. A simplified description of the stresses in the powder and in the container is proposed and used to demonstrate that the axial shrinkage of the powder is always smaller than the radial shrinkage, as observed by McCoy *et al.* (1985) and McCoy and Wills (1987) in an alumina powder and by Wadley *et al.* (1990) in copper, when thermo-elastic effects can be neglected. Finally, the simplified model is compared with results obtained by finite element calculations. This comparison validates the assumptions of the proposed simplified model.

GEOMETRY AND STRESSES

We assume that the cylindrical container can be divided in two different parts: (1) the side [denoted by (')], (2) the top ('). The powder (^{p}) is represented by a cylindrical core enclosed in the container. We use the cylindrical coordinates (r, θ, z). The geometry of the container is shown in Fig. 1. We further assume that the stresses and strain rates are uniform in each part. The stress tensor in the powder can then be expressed as:

$$\bar{\sigma}^p = \begin{pmatrix} \sigma^p_{rr} & 0 & 0 \\ 0 & \sigma^p_{rr} & 0 \\ 0 & 0 & \sigma^p_{zz} \end{pmatrix}. \tag{1}$$

In the side part of the container, at the interface between the powder and the dense wall, the stress tensor is expressed as:

† Present address: UC Santa Barbara, Materials Department, Santa Barbara, CA 93106, U.S.A.
‡ Present address: CICE SA, 63 rue Beaumarchais, 93104 Montreuil, France.

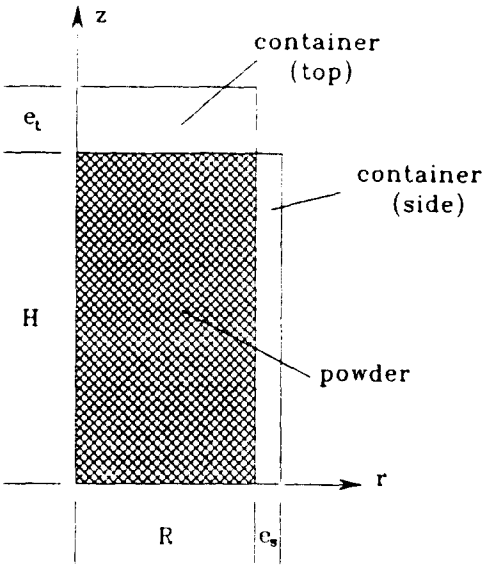

Fig. 1. Geometry of the proposed model.

$$\tilde{\sigma}^s = \begin{bmatrix} \sigma^s_{rr} = \sigma^p_{rr} & 0 & 0 \\ 0 & \sigma^s_{\theta\theta} = \dfrac{\sigma_h(R+e_s) - \sigma^s_{rr}R}{e_s} & 0 \\ 0 & 0 & \sigma^s_{zz} \end{bmatrix}. \tag{2}$$

The continuity of the stress vector ($\tilde{\sigma}\mathbf{n}$) at the interface between the two materials implies $\sigma^s_{rr} = \sigma^p_{rr}$. $\sigma^s_{\theta\theta}$ is computed assuming that the container can be represented by a thin shell of thickness e_s loaded with an external pressure equal to $-\sigma_h$ and can internal pressure equal to $-\sigma^p_{rr}$. It should be noted that if $\sigma^p_{rr} = \sigma_h$, the hoop stress in the container is also equal to σ_h. Finally, the stress tensor in the upper part of the container, at the interface between the two materials, is given by:

$$\tilde{\sigma}^t = \begin{pmatrix} \sigma^t_{rr} & 0 & 0 \\ 0 & \sigma^t_{rr} & 0 \\ 0 & 0 & \sigma^p_{zz} \end{pmatrix}. \tag{3}$$

The different assumptions made on the stress state in each part are summarized in Fig. 2. The temperature is supposed to be uniform in the container.

FLOW IN THE POWDER

The powder is described by a continuous medium with the relative density as an internal variable. Following Shima and Oyane (1976) and Abouaf *et al.* (1989), we may use an equivalent stress defined as:

$$\sigma^2_{eq} = 3c(\rho)J_2 + f(\rho)I_1^2$$

$$\text{with} \quad \begin{cases} I_1 = Tr(\tilde{\sigma}) = \sigma_{11} + \sigma_{22} + \sigma_{33} \\ J_2 = \frac{1}{2}\tilde{s} : \tilde{s} \\ \tilde{s} = \tilde{\sigma} - \frac{1}{3}I_1\tilde{1}. \end{cases} \tag{4}$$

c and f are assumed to be two functions of the relative density ρ and represent the stress localization induced by the porosity. I_1 and J_2 are respectively the first and second invariants

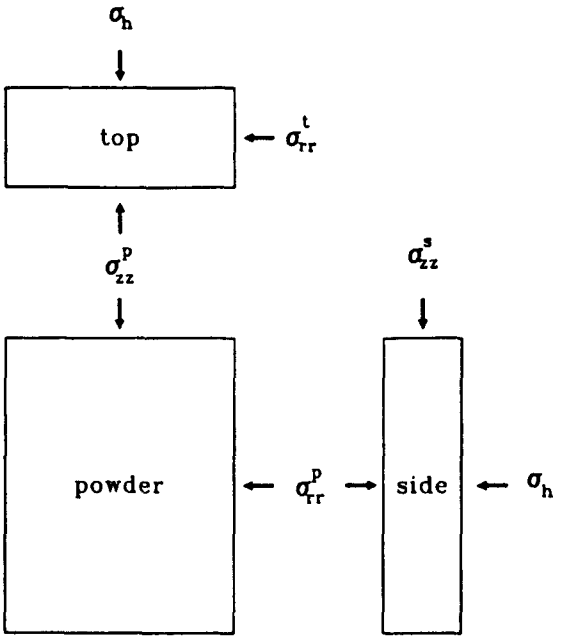

Fig. 2. Stresses acting on the different parts of the cylinder.

of the stress tensor (i.e. pressure and shear); $\tilde{1}$ is the unitary second order tensor. Assuming a normality rule between the visco-plastic potential and the strain rate tensor, and using the following definition of the equivalent strain rate $\dot{\varepsilon}_{eq}$ (Shima and Oyane, 1976)

$$\rho \dot{\varepsilon}_{eq} \sigma_{eq} = \tilde{\sigma} : \dot{\tilde{\varepsilon}}_{vp} \tag{5}$$

it becomes possible to calculate the visco-plastic strain rate tensor $\dot{\tilde{\varepsilon}}_{vp}$:

$$\dot{\tilde{\varepsilon}}_{vp} = \rho \frac{\dot{\varepsilon}_{eq}}{\sigma_{eq}} \left(\tfrac{1}{2} c \tilde{s} + f I_1 \tilde{1}\right). \tag{6}$$

$\dot{\varepsilon}_{eq}$ is given by the flow equation of the material and can be usually expressed as: $\dot{\varepsilon}_{eq} = F(\sigma_{eq}, T, a_i, \ldots)$, a_i representing internal parameters such as grain size, T the temperature. According to eqns (1) and (6), $\dot{\tilde{\varepsilon}}^p_{vp}$ is given by (for the sake of simplicity, we will take a vectorial notation for all tensors, since they are all diagonal):

$$\dot{\tilde{\varepsilon}}^p_{vp} = \rho \left(\frac{\dot{\varepsilon}_{eq}}{\sigma_{eq}}\right)^p \begin{bmatrix} \frac{c}{2}(\sigma^p_{rr} - \sigma^p_{zz}) + f(2\sigma^p_{rr} + \sigma^p_{zz}) \\ \frac{c}{2}(\sigma^p_{rr} - \sigma^p_{zz}) + f(2\sigma^p_{rr} + \sigma^p_{zz}) \\ c(\sigma^p_{zz} - \sigma^p_{rr}) + f(2\sigma^p_{rr} + \sigma^p_{zz}) \end{bmatrix}. \tag{7}$$

FLOW IN THE CONTAINER

The flow in the container (using usual visco-plastic laws for dense materials) is given by (in the side part):

$$\dot{\bar{\varepsilon}}^s_{cp} = \frac{1}{2}\left(\frac{\dot{\varepsilon}_{eq}}{\sigma_{eq}}\right)^s \begin{pmatrix} \sigma^p_{rr}(2+\eta) & - & \sigma_h(1+\eta) & - & \sigma^s_{zz} \\ -\sigma^p_{rr}(1+2\eta) & + & 2\sigma_h(1+\eta) & - & \sigma^s_{zz} \\ -\sigma^p_{rr}(1-\eta) & - & \sigma_h(1+\eta) & + & 2\sigma^s_{zz} \end{pmatrix} \tag{8}$$

with

$$\eta = \frac{R}{e_s}. \tag{9}$$

In the top part the strain rate tensor is given by:

$$\dot{\bar{\varepsilon}}^t_{cp} = \frac{\sigma^t_{zz} - \sigma^t_{rr}}{2}\left(\frac{\dot{\varepsilon}_{eq}}{\sigma_{eq}}\right)^t \begin{pmatrix} -1 \\ -1 \\ 2 \end{pmatrix}. \tag{10}$$

COMPATIBILITY AND EQUILIBRIUM

The continuity of displacement at the interface between the powder and the container gives the following relations

$$\begin{aligned} \mathbf{U}^p(r = R) &= \mathbf{U}^s(r = R) \\ U^p_r(r) &= U^t_r(r) \quad \forall r \end{aligned} \tag{11}$$

where $\mathbf{U}$ is the displacement, with components U_r and U_z along the radial and axial axis. This system is equivalent to

$$\begin{aligned} \dot{\varepsilon}^p_{\theta\theta} &= \dot{\varepsilon}^s_{\theta\theta} = \dot{\varepsilon}^t_{\theta\theta} \\ \dot{\varepsilon}^p_{zz} &= \dot{\varepsilon}^s_{zz}. \end{aligned} \tag{11'}$$

The equilibrium of forces along the Oz axis (inside and outside the container) is expressed by the following equations:

$$\int_0^{R+e_s} \sigma_{zz} r \, dr = R^2\sigma^p_{zz} + [(R+e_s)^2 - R^2]\sigma^s_{zz} = (R+e_s)^2\sigma_h. \tag{12}$$

Therefore we obtain a system of four equations with four unknown quantities, σ^p_{rr}, σ^p_{zz}, σ^s_{zz}, σ^t_{rr}, which can be numerically solved using an iterative Newton–Raphson method. Equations (7), (8) and (10) are then integrated to obtain the evolution of the different parameters during the HIP Process. The thickness of the container is updated assuming that the volume of the dense material remains constant in each part.

AXIAL/RADIAL DEFORMATION OF THE POWDER

It is now well established experimentally that the radial deformation of a powder compact enclosed in a dense container and subjected to a HIP cycle is greater than its axial deformation (McCoy *et al.*, 1985). We will now demonstrate this observed trend using the preceding equations. The behaviour of the top part of the container is of minor interest, and we shall focus on the interface between the powder and the side part of the container. We will use normalized stresses: $\Pi^p_{zz} = \sigma^p_{zz}/\sigma_h, \ldots$ Equations (11') and (12) become (in this part we will neglect elastic effects which are of minor interest during the densification of the powder):

$$\Pi^p_{rr}(c/2+2f)+\Pi^p_{zz}(f-c/2)=\kappa[-\Pi^p_{rr}(1+2\eta)+2(1+\eta)-\Pi^s_{zz}] \tag{13a}$$

$$\Pi^p_{rr}(2f-c)+\Pi^p_{zz}(c+f)=\kappa[-\Pi^p_{rr}(1-\eta)-(1+\eta)+2\Pi^s_{zz}] \tag{13b}$$

$$\eta^2\Pi^p_{zz}+(1+2\eta)\Pi^s_{zz}=(1+\eta)^2 \tag{13c}$$

with

$$\kappa=\frac{1}{2\rho}\frac{(\dot\varepsilon_{eq}/\sigma_{eq})^s}{(\dot\varepsilon_{eq}/\sigma_{eq})^p}.$$

Using eqn (13c), Π^s_{zz} can be expressed as a function of Π^p_{zz}

$$\Pi^s_{zz}=\frac{(1+\eta)^2-\eta^2\Pi^p_{zz}}{1+2\eta} \tag{14}$$

and eqns (13a) and (13b) can be rewritten as

$$\Pi^p_{rr}[c/2+2f+(1+2\eta)^2\kappa']+\Pi^p_{zz}[f-c/2-\kappa'\eta^2]=\kappa'(1+\eta)(1+3\eta) \tag{15a}$$

$$\Pi^p_{rr}[2f-c+(1-\eta)(1+2\eta)\kappa']+\Pi^p_{zz}[c+f+2\kappa'\eta^2]=\kappa'(1+\eta) \tag{15b}$$

with $\kappa'=\kappa/(1+2\eta)$.

Since κ' depends on both Π^p_{rr} and Π^p_{zz}, the preceding equations are not linear. However, we will solve them as if they were linear (i.e. κ' is independent of Π^p_{rr} and Π^p_{zz}). Propositions which are true for all $\kappa'>0$ will also be true for the non-linear solution of eqn (15). Considering κ' as constant, the solution is therefore

$$\Pi^p_{rr}=\frac{3\kappa'}{\Delta}(1+\eta)\left[(1+2\eta)\left(\frac{c}{2}+\eta^2\kappa'\right)+\eta f\right] \tag{16a}$$

$$\Pi^p_{zz}=\frac{3\kappa'}{\Delta}(1+\eta)\left[(1+2\eta)\left(\frac{c}{2}+\eta^2\kappa'\right)-2\eta f\right] \tag{16b}$$

$$=\Pi^p_{rr}-9\eta f\frac{\kappa'}{\Delta}(1+\eta)=\Pi^p_{rr}-\delta\Pi.$$

Δ is equal to

$$\Delta=\tfrac{9}{2}fc+\kappa'[\tfrac{1}{2}c+\tfrac{9}{2}(c+\tfrac{2}{3}f)\eta+3(c+4f)\eta^2]+3\kappa'^2\eta^2(1+2\eta)(1+\eta). \tag{17}$$

Since η, κ, c and f have positive values, Δ is always positive. Therefore $\Pi^p_{zz}<\Pi^p_{rr}$. According to eqn (16a) $\Pi^p_{rr}>0$; and Π^p_{zz} can be rewritten as:

$$\Pi^p_{zz}=\frac{3\kappa'}{\Delta}(1+\eta)\left[\frac{c}{2}+\eta(c-2f)+\eta^2\kappa'(1+2\eta)\right]. \tag{18}$$

Since $c>2f$,† $\Pi^p_{zz}>0$. Now we have

$$\Delta-\Delta\Pi^p_{rr}=9\left[\frac{fc}{2}+f\eta^2\kappa'\right]>0, \tag{19}$$

therefore $\Pi^p_{rr}<1$ and since $\Pi^p_{zz}<\Pi^p_{rr}<1$, $\Pi^s_{zz}>1$ according to eqn (14). Finally, we get:

† It can be easily shown that the property $c>2f$ must be verified by the material: consider a porous cylinder tested under compressive uniaxial load. According to eqn (6), the radial strain rate is proportional to $(f-c/2)\sigma_{zz}$, with $\sigma_{zz}<0$. Under a compressive load, the radial strain is expected to be positive (Bordia and Scherer, 1985) and therefore $c>2f$.

$$0 \leqslant \Pi^p_{zz} \leqslant \Pi^p_{rr} \leqslant 1 \leqslant \Pi^v_{zz}. \tag{20}$$

Now if we consider the left-hand side of eqns (13a) and (13b), we obtain:†

$$\dot{\varepsilon}^p_{rr} \propto^+ \sigma_h[c/2(\Pi^p_{rr} - \Pi^p_{zz}) + f(2\Pi^p_{rr} + \Pi^p_{zz})] \tag{21a}$$

$$\dot{\varepsilon}^p_{zz} \propto^+ \sigma_h[c(\Pi^p_{zz} - \Pi^p_{rr}) + f(2\Pi^p_{rr} + \Pi^p_{zz})]. \tag{21b}$$

Since $\sigma_h < 0$, $\dot{\varepsilon}^p_{rr} < 0$. Using eqn (16), $\dot{\varepsilon}^p_{zz}$ can be rewritten as:

$$\dot{\varepsilon}^p_{zz} \propto^+ \sigma_h \frac{3\kappa' f(1+\eta)}{\Delta}[3\eta^2\kappa'(1+2\eta) + \tfrac{1}{2}c]. \tag{22}$$

This relation shows that $\dot{\varepsilon}^p_{zz} < 0$. The difference between the radial and the axial strain rate is given by:

$$(\dot{\varepsilon}^p_{rr} - \dot{\varepsilon}^p_{zz}) \propto^+ \tfrac{1}{2}c\sigma_h[\Pi^p_{rr} - \Pi^p_{zz}] < 0. \tag{23}$$

Finally, we obtain the following relations for the strain rates:

$$\dot{\varepsilon}^p_{rr} \leqslant \dot{\varepsilon}^p_{zz} \leqslant 0. \tag{24}$$

Therefore this proves (since it has been demonstrated for all κ) that the radial shrinkage is always greater than the axial one during HIP processing of cylindrical containers.

One parameter which characterizes the inhomogeneity of the powder deformation is the difference between the axial and radial stresses $\delta\Pi = \Pi^p_{rr} - \Pi^p_{zz}$. If the container deforms much more easily than the powder, κ has a high value ($\kappa \gg 1$)

$$\text{for high } \kappa \quad \begin{aligned} &\Delta \sim 3\kappa^2\eta^2 \frac{1+\eta}{1+2\eta} \\ &\text{and } \delta\Pi \sim \frac{3f}{\kappa\eta} \to 0 \quad \Pi^p_{rr} \to 1. \end{aligned} \tag{25}$$

If the container thickness is small compared to the radius ($\eta \gg 1$):

$$\text{for high } \eta \quad \begin{aligned} &\Delta \sim \tfrac{1}{2}\kappa^2\eta^2 \\ &\text{and } \delta\Pi \sim \frac{3f}{\kappa\eta} \to 0 \quad \Pi^p_{rr} \to 1. \end{aligned} \tag{26}$$

This means that a highly deformable container or a thin wall thickness will achieve more homogeneously deformed cylinders.

Note. The preceding results can be generalized in the case of isotropic pressure sensitive materials independent of the third invariant of the stress tensor. If it is possible to find $A > 0$ and $B > 0$ functions of first and second invariant and internal parameters, so that the strain rate tensor can be expressed as

$$\dot{\tilde{\varepsilon}}_{vp} = A\tilde{s} + BI_1\tilde{1}, \tag{27}$$

it is therefore possible to find for each stress and density state parameters f and c such that the preceding equation is equivalent to eqn (6), and the preceding results can also be applied.

† The relation $A \propto^+ B$ means that A is proportional to B and that $A \cdot B \geqslant 0$.

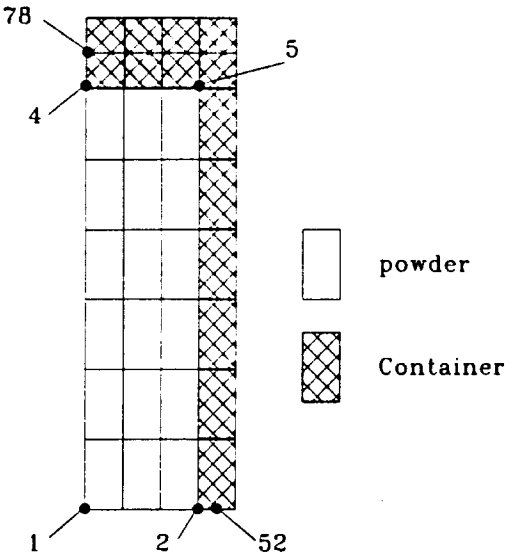

Fig. 3. Mesh used for the finite element computation.

COMPARISON WITH FINITE ELEMENT RESULTS

Compatibility and equilibrium equations are solved using the Newton–Raphson method; constitutive equations are integrated using an implicit scheme. The thermo-elastic behaviour is also taken into account and the increment of elastic strain is given by

$$\delta\tilde{\varepsilon}_e = C^{-1}_{T+\delta T,\rho}(\tilde{\sigma}+\delta\tilde{\sigma}) - C^{-1}_{T,\rho}\tilde{\sigma} + (\alpha_{T+\delta T}(T+\delta T) - \alpha_T T)\tilde{1} \tag{28}$$

where δ denotes the increment, C is the elasticity tensor, α the thermal expansion coefficient and T the temperature. It should be noted that for the calculation of C (which depends on both temperature and density) the relative density is supposed to be constant during the increment. This simplifies the calculation with little effect on accuracy since the relative density change remains small during each time increment.

The finite element calculations were performed using the Zébulon program developed by the Centre des Matériaux de l'École des Mines de Paris. The method has been presented in earlier papers (Abouaf *et al.*, 1989; Besson and Abouaf, 1989). The mesh which has been employed is shown in Fig. 3. The nodes used for the comparison of the two sets of calculation are also shown in this figure. It should be noted that nodal values of stresses are extrapolated from values at Gaussian points. Locations of these nodes were chosen to be representative of the simple assumptions made on stresses and geometry.

The following parameters were used for the computation:

- Container (304L stainless steel). See Dadras (1985) for creep and Hoke (1977) for plastic behaviour and thermo-elastic parameters.
- Powder:

$$\dot{\varepsilon}_{eq} = 31.2\,10^6 \exp(-419000/RT)\sigma_{eq}$$

$$f = 80(1-\rho) \quad \text{and} \quad c = 1+160(1-\rho).$$

  This is a simplified version of the constitutive equations proposed for alumina in an earlier paper (Besson and Abouaf, 1989). The initial relative density is equal to 0.51.
- the HIP cycle is the following:

Time (s)	0	3840	14,640	20,000
Pressure (MPa)	16	50	50	0
Temperature (°C)	27	1300	1300	27

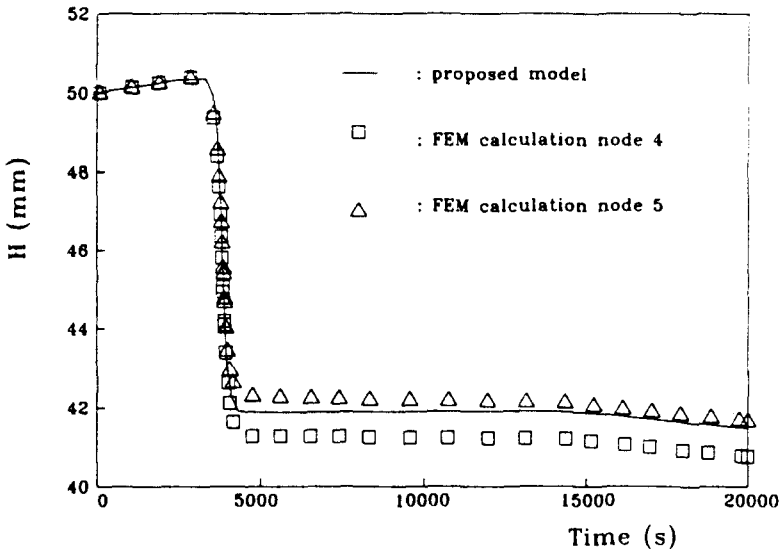

Fig. 4. Variation of the height of the powder cylinder.

- Initial dimensions

$$\begin{cases} H = 50 \text{ mm} \\ R = 20 \text{ mm} \\ e_s = e_t = 5 \text{ mm}. \end{cases}$$

Comparison between the FEM calculation and the proposed model gives the following trends:

(a) Variations of dimensions: Fig. 4 represents, as a function of time, the variation of the height of the porous cylinder. The simplified model gives a height which lies between the height at node 4 (centre) and node 5 (upper corner) as would have been expected since the model does not take into account the corner effect (barreling of the cylinder). The same remarks can be made on the variation of the radius at nodes 2 and 5 (Fig. 5).

(b) Stresses in the powder: radial and axial stresses in the powder compact are compared in Figs 6 and 7. Good agreement between FEM computation and the simplified model is found. The decrease of stresses during the heating phase corresponds to the

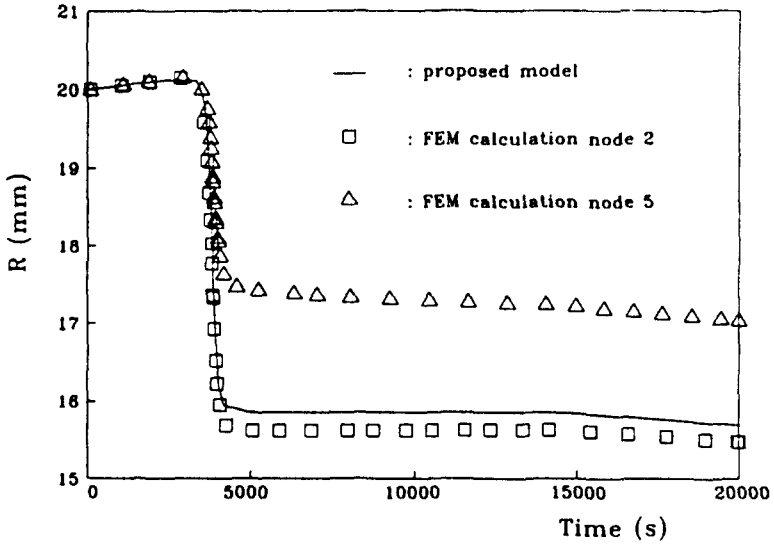

Fig. 5. Variation of the radius of the powder cylinder.

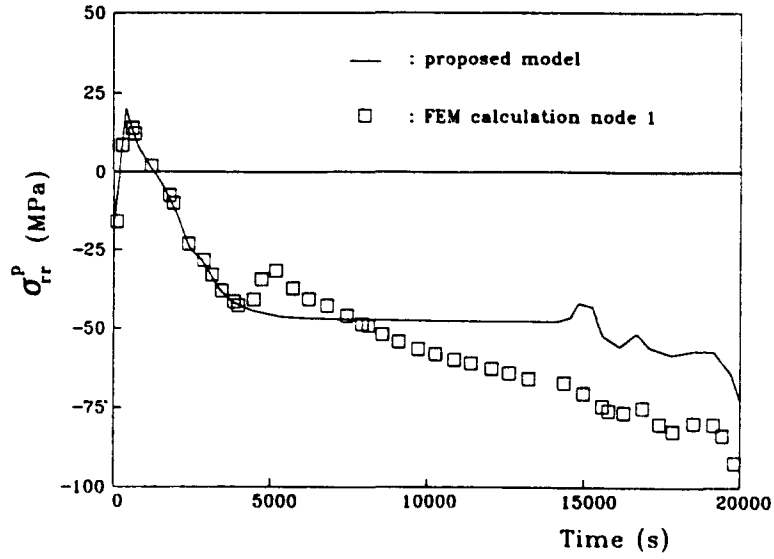

Fig. 6. Radial stress in the powder (σ_{rr}^{p}).

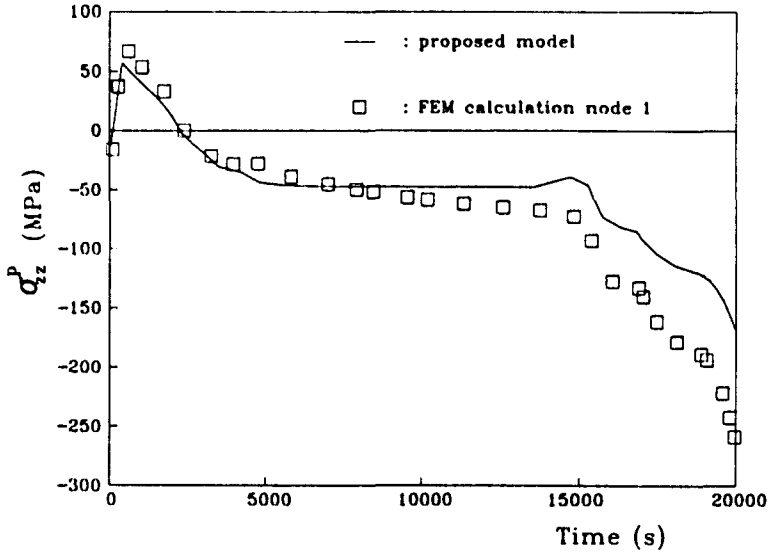

Fig. 7. Axial stress in the powder (σ_{zz}^{p}).

plastification of the container due to thermal expansion mismatch between the powder and the container. Plastification is also observed during the cooling phase. As shown in Fig. 8 the relation $0 \leqslant \Pi_{zz}^{p} \leqslant \Pi_{rr}^{p} \leqslant 1$ is actually observed during the densification process. This is not true during the heating phase during which elastic effects are more important than visco-plastic ones. It should be noted that the simplified analysis neglects thermo-elastic effects. It is also worth noting that the shield effect of the container is not negligible since the radial and axial stresses in the powder are significantly smaller than the applied HIP pressure.

(c) Stresses in the container: axial and hoop stresses in the container (side) are compared in Figs 9 and 10. The same remarks as in the case of the stresses in the powder can be made. Good agreement between the two different computations is also found.

EFFECT OF GEOMETRY AND RHEOLOGY ON THE DEFORMATION OF THE POROUS BODY

The simplified model can be used to rapidly estimate† the different effects of the geometry and the rheology on the deformation of the porous cylinder. To compare

† It takes approximately 30 min to run the program on an AT IBM computer without math-coprocessor.

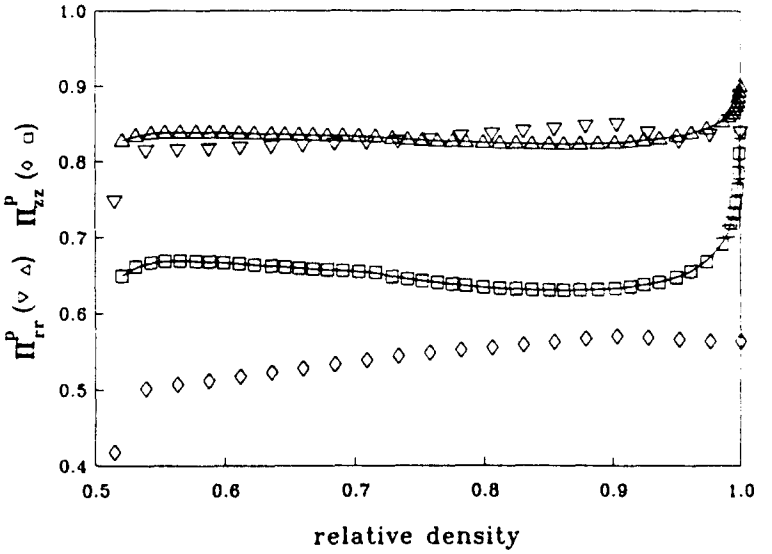

Fig. 8. Normalized radial and axial stresses (Π^p_{rr} and Π^p_{zz}) in the powder during densification (simplified model): Π^p_{rr} △ (simplified model), ▽ (FEM), Π^p_{zz} □ (simplified model) ◇ (FEM). The FEM results correspond to node 1.

the different calculations, we use the following factor (introduced by McCoy *et al.*, 1985):

$$k = \frac{\ln (H/H_0)}{\ln (R/R_0)} \tag{29}$$

where H_0 and R_0 are respectively the initial height and radius of the cylinder. If densification is isotropic, k is equal to 1. In most cases k is smaller than 1, since radial shrinkage is greater than axial shrinkage. Unless otherwise specified, the same parameters as in the previous section are used for these computations. The following trends have been observed:

(a) *Comparison with FEM calculation*: in the case of FEM results, k is calculated using displacement of nodes 2 and 4. Two different wall thickness were used with $e_s = e_t$. Good agreement is found between the two calculations.

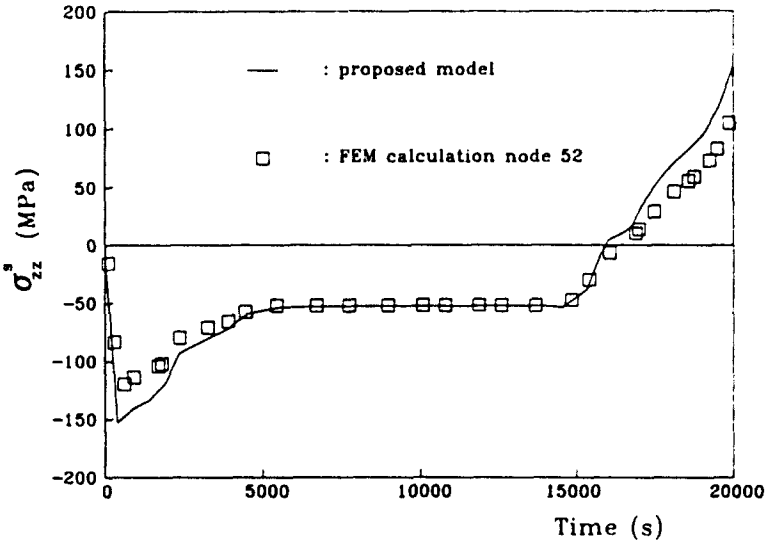

Fig. 9. Axial stress in the container (side) (σ^s_{zz}).

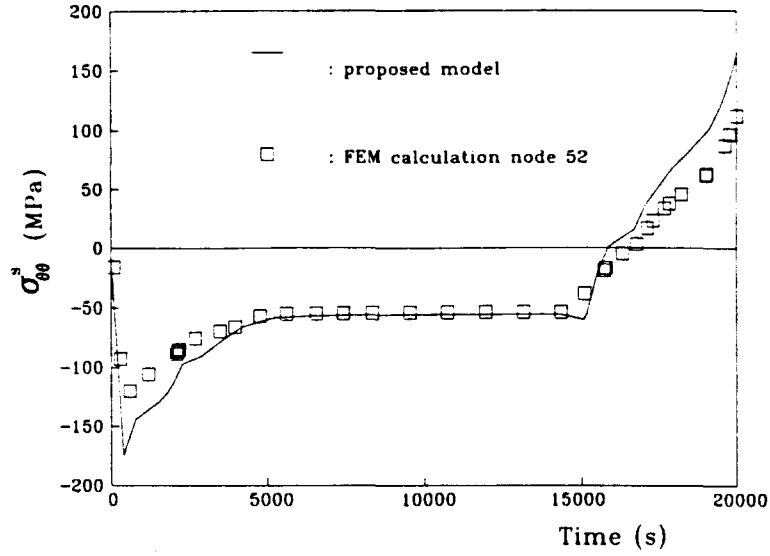

Fig. 10. Hoop stress in the container (side) ($\sigma'_{\theta\theta}$).

Thickness (mm)	k simplified model	k FEM result
5	0.771	0.796
2	0.901	0.931

McCoy *et al.* (1985) experimentally found $k \simeq 0.85$ for an alumina powder enclosed in a stainless steel container with a ratio $R/e_s \simeq 7$. This value is in good agreement with our computations. The result of McCoy *et al.* (1985) can hardly be explained by the presence of a temperature gradient (since the heating rate is small), and is probably related to the presence of a relatively thick container.

(b) *Effect of thickness*: k increases when the wall thickness is decreased ($e_s = e_t$).

Thickness (mm)	1	2	5	10
k	0.949	0.901	0.771	0.622

(c) *Effect of the ratio f/c*: for this set of calculations the parameter c is constant ($c = 1 + 160(1-\rho)$) and the parameter f is given by the following formula: $f = (c-1)/\omega$, with different values of ω. When ω increases, the factor k decreases: this can be explained by the fact that densification becomes more and more difficult for a given shear behaviour (smaller f for a given c).

ω	2	4	8	16	32
k	0.771	0.663	0.535	0.408	0.303

(d) *Effect of the creep rate of the container*: the creep rate of the container was multiplied by 10 and 0.1.

Creep rate multiplied by	×0.1	×1	×10
k	0.699	0.771	0.933

The higher the creep rate, the more homogeneous the deformation. For a given creep behaviour of the container, a highly deformable powder will trigger a more inhomogeneous deformation.

CONCLUSION

Anisotropic densification of porous cylinders during HIP, when temperature is homogeneous, can be explained by a mechanical interaction between the powder and the container. The simplified model shows that (taking absolute values) the radial stress in the powder is always greater than the axial stress and that both are smaller than the external HIP pressure. Therefore the stress state in the powder is not hydrostatic. It can then be shown that the radial shrinkage of the powder is always greater than the axial shrinkage. If a dense skin is formed at the hotter (external) surface of the powder, due to slow heat transfer, this skin will act exactly as a container of high stiffness and generate inhomogeneous deformation. Results obtained by a simplified computer model are in good agreement with the trends observed by McCoy *et al.* (1985) and are validated by more accurate results calculated using a FEM simulation.

Acknowledgement—This work was partially supported by the NSF grant DMR-87-13919 to the University of California, Santa Barbara Materials Department.

REFERENCES

Abouaf, M., Chenot, J. L., Raisson, G. and Bauduin, P. (1989). Finite element simulation of hot isostatic pressing of metal powders. *Int. J. Numer. Meth. Engng* **2**, 191–212.

Besson, J. and Abouaf, M. (1989). Finite element simulation of hot isostatic pressing of ceramic powders. Paper presented at the 2nd Int. Conf. on HIP: Theory and Application, Gaithersburg, June 1989.

Bordia, R. K. and Scherer, G. W. (1988). On constrained sintering—II. Comparison of constitutive models. *Acta Met.* **36**, 2399–2409.

Dadras, P. (1985). Flow stress equations of type 304L stainless steel and AISI 1055 steels. *J. Engng Mater. Technol.* **107**, 97–100.

Hoke, J. H. (1977). *Handbook of Stainless Steel* (Edited by D. Peckner and I. M. Bernstein), Chapter 21. McGraw-Hill, New York.

Li, W. B., Ashby, M. F. and Easterling, K. E. (1987). On densification and shape change during hot isostatic pressing. *Acta Met.* **35**, 2831–2842.

McCoy, J. K., Muttart, L. E. and Wills, R. R. (1985). Continuous monitoring of volumetric changes in ceramic powder compacts during hot isostatic pressing. *Am. Ceram. Soc. Bull.* **64**, 1240–1244.

McCoy, J. K. and Wills, R. R. (1987). Densification by interface-reaction controlled grain-boundary diffusion. *Acta Met.* **35**, 577–585.

Shima, S. and Oyane, M. (1976). Plasticity theory for porous metals. *Int. J. Mech. Sci.* **18**, 285–291.

Wadley, H. N., Schaefer, R. J., Kahn, A. H., Ashby, M. F., Clough, R. B., Geffen, Y. and Wlassich, J. J. (1990). To be published.